Metal−Phosphorus Bonding in Complexes $W@Au_{12}PX_3$ (X = H, F, Cl, Br, I, Me, OMe) and $[M@Au_{12}]^qPH_3$ ($M^q = Hf^{2-}$, Ta^-, W, Re^+, Os^{2+}, Ir^{3+}, Pt^{4+}, Au^{5+}): Relativistic DFT Investigations

Jia Li, Yi-Xiang Qiu, and Shu-Guang Wang*

School of Chemistry and Chemical Technology, Shanghai Jiao Tong University, 200240 Shanghai, China

Received: September 22, 2008; Revised Manuscript Received: December 18, 2008

Relativistic density functional theory (DFT) calculations of the geometries and Au−P bonding of $W@Au_{12}PX_3$ (X = H, F, Cl, Br, I, Me, OMe) and $[M@Au_{12}]^qPH_3$ ($M^q = Hf^{2-}$, Ta^-, W, Re^+, Os^{2+}, Ir^{3+}, Pt^{4+}, Au^{5+}) have been carried out. There are some regular changes in geometry and binding of these two kinds of complexes with the variation of the phosphanes PX_3 and transition metals M^q. The energy decomposition analysis confirms that the PX_3 ligands are σ donors. The donor tendency ($\Delta E_\sigma/\Delta E_\pi$) decreases for different X with increasing electronegativity and for different M^q from Au^{5+} to Hf^{2-}, while the π-back-donation increases in the same direction. The calculated P−H bond lengths show a regular decrease from Hf^{2-} to Ir^{3+}, but have abnormal trends for Pt^{4+} and Au^{5+}.

1. Introduction

Gold clusters and nanoparticles had become an active research field ten years ago because of the discovery of their remarkable catalytic properties[1−3] and potential application in nanoelectronics, nanosensors, and as biological markers.[4] Among all kinds of gold clusters, those with compact closed structures and "magic numbers" of atoms (13, 38, 55, etc.) have more often been investigated because of their unusually high stabilities.[5−7] Pyykkö and Runeberg first predicted the existence of the closed-shell cluster $W@Au_{12}$ as a derivative of Au_{13}.[8] They suggested an unusual stability due to three complementary reasons, namely, relativistic effects,[9] aurophilic attraction,[10] and perfect 18-electron shell structure of the central tungsten atom.[11,12] Shortly thereafter, the system was experimentally prepared by Li et al.[13] It formed spontaneously from the metal vapors injected to a helium carrier gas. Theoretical calculations and the experimental data supported the originally suggested icosahedral (I_h) structure. Therefore, the isoelectronic derivatives of $W@Au_{12}$, $[M@Au_{12}]^q$ ($M^q = Hf^{2-}$, Ta^-,[14] W, Re^+, Os^{2+}, Ir^{3+}, Pt^{4+}, Au^{5+}), which are the smallest clusters with an inner atom were examined as a first step toward an understanding of the catalytic activities of Au catalysts, by using quantum chemical calculations.

Phosphanes PX_3 belong to the most ubiquitous ligand in transition metal chemistry. Besides being applied in academic research, metal complexes with phosphane ligands have been used as powerful catalysts in homolytically catalyzed chemical reactions that are important for industrial purposes. The steric and electronic properties of PX_3 complexes can be modulated within a broad range by the variation of the atom or group X. To modify the properties of the complexes, it is helpful to understand the nature of the Au−PX_3 interactions.

Chemical bonding between a Lewis acid and a Lewis base is usually described in terms of donor−acceptor interactions between the occupied orbital of the donor and the vacant orbital of the acceptor. The generally accepted bonding model,[15] first suggested by Dewar[16] and later elaborated by Chatt and Duncanson,[17] focuses on donor→acceptor σ-donation and acceptor→donor π-back-donation. Figure 1 shows, as an example of the Dewar−Chatt−Duncanson (DCD) model, the orbital interactions between a $W@Au_{12}$ cluster Lewis acid and a PH_3 Lewis base.

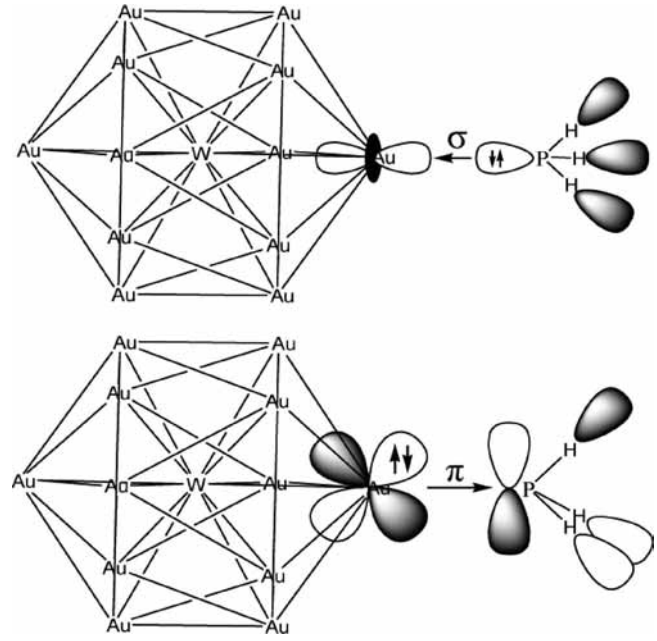

Figure 1. Schematic representation of the $W@Au_{12}PH_3$ orbital interactions. Au←PH_3 σ-donation (top) and Au→PH_3 π-back-donation (bottom).

During the past few decades the nature of the metal−phosphorus bonding has been the focus of several theoretical studies[18−25] and was investigated by a variety of experimental techniques.[26,27] However, there are still some controversial discussions of the results that were obtained so far, in particular with respect to the role of M→P back-bonding and the possible bonding mechanisms as well as about the σ and π contributions to the bond. The strength of the M→PX_3 π-back-donation has also been estimated from NMR spectroscopic data. Wang et al. measured the oxygen-17 quadrupole constants of $(CO)_5WPR_3$

* Corresponding author.

10.1021/jp808403u CCC: $40.75
Published on Web 01/29/2009

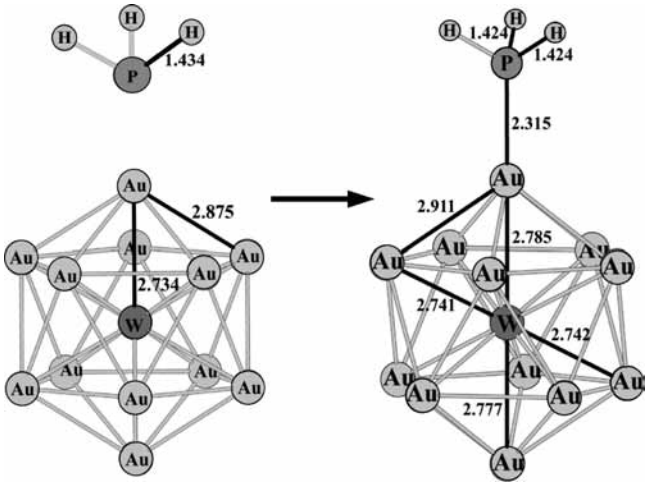

Figure 2. Geometries of free PH_3, W@Au_{12}, and W@$Au_{12}PH_3$. The most important optimized bond lengths (in Å) are shown.

complexes and came to the conclusion that PMe_3 is a stronger π-acceptor ligand than NMe_3 but weaker than $P(OMe)_3$.[26] Alyea et al. reported experimental ^{95}Mo, ^{31}P, and ^{13}C NMR chemical shifts of $M(CO)_{6-n}L_n$ ($n = 1-3$) complexes.[27] According to these results PCl_3 appears as a weak π-acceptor. However, a recent theoretical study of the ^{95}Mo and ^{31}P NMR chemical shifts of $(CO)_5MoPR_3$ by Ziegler et al. showed that PCl_3 is actually a very strong π-acceptor that is stronger than PF_3 and, particularly, PH_3 and PMe_3.[18] There was the another trend in the work of Frenking et al. studying $M(CO)_5PX_3$ complexes (M = Cr, Mo, W).[25] They concluded the order $PF_3 > PCl_3 > PMe_3 > PH_3$ for the π-bonding contributions to the M−PX_3 bonds, which was given by the absolute values of ΔE_π and by the relative strengths given as percent ΔE_π.

In this paper, the coordination bonding in the complexes of type W@$Au_{12}PX_3$ (X = H, F, Cl, Br, I, Me, OMe) and of isoelectronic type [M@Au_{12}]$^q PH_3$ ($M^q = Hf^{2-}$, Ta^-, W, Re^+, Os^{2+}, Ir^{3+}, Pt^{4+}, Au^{5+}) is our main interest. Most previous theoretical studies that analyzed the M−L bonds focused on neutral complexes. However, M can also be negatively or positively charged. In recent years, M−L complexes that carry negative or positive charges have been intensively investigated both experimentally[28] and theoretically.[29−33] And it is most important that we can here vary both the donor and acceptor strengths.

Quantum chemical calculations of geometries and bond dissociation energies and theoretical analyses of bonding in W@$Au_{12}PX_3$ and [M@Au_{12}]$^q PH_3$ were carried out by using gradient-corrected density functional theory. We analyzed the electronic structure and the energy of the Au−P bonds. The changes in the σ and π charges were investigated by NBO[34] population analysis. The strength of the σ and π contributions to the orbital interactions has been determined by EDA[35,36] (energy decomposition analysis), which often has been used to analyze bonding.[37,38]

2. Computational Details

All calculations have been done with the ADF2004 program.[39] The local spin density approximation (LSD)[40] with the correlation correction of Vosko et al. (VWN)[41] and the gradient corrections to exchange and correlation developed by Perdew and Wang (PW91)[42,43] have been used. Scalar relativistic effects have been considered at the level of the zero-order regular approximation (ZORA).[44] Slater-type-orbital (STO) basis sets of triple-ζ plus double polarization quality (TZ2P) have been used for all atoms.[45] The small inner core shells up to 4f were calculated by the Dirac method[46] and kept frozen for all 6-row metal elements; the 5s, 5p, 5d, and 6s shells were treated as valence shells. Present day DFT-GGA approaches usually give too long equilibrium distances between two heavy atoms but can predict reasonable energies. In this paper we want to restrict our discussion on the interaction between Au and P atoms and the trends upon changing the ligand. So we still use the DFT-GGA approaches for all of our calculations. Frequency analyses were carried out to confirm the stability of the obtained structures. For further elucidation an NBO analysis has been performed (PW91-DFT level, SDD,[47] and 6-31g* [48] basis sets for the metal and the other atoms, respectively) with Gaussian03.[49]

3. Results and Discussion

3.1. Energy Decomposition Analysis Method. The standard definition of the bond energy ΔE_b between two fragments A−B is

$$\Delta E_b = E_{AB} - E_A - E_B$$

Within the EDA method, the bond energy between the two fragments [M@Au_{12}]^q and PX_3 is decomposed into two contributions:

$$\Delta E_b = \Delta E_{prep} + \Delta E_{int}$$

ΔE_{prep} is the energy change of fragments A and B from isolated equilibrium structure to the structure in compound A−B. ΔE_{int} is the interaction energy between the two fragments in the molecule. The latter quantity will be the focus of the present work since ΔE_{prep} turned out to be small. The interaction energy ΔE_{int} can be divided into three main components:

$$\Delta E_{int} = \Delta E_{pauli} + \Delta E_{elstat} + \Delta E_{orb}$$

ΔE_{pauli} gives the repulsive interaction between the overlapping fragments in the molecule caused by the fact that two electrons of the same spin cannot occupy the same region in space. ΔE_{elstat} gives the electrostatic interaction of the electron density distributions of the fragments. Finally, the orbital interaction term ΔE_{orb} represents the stabilization produced when the fragment orbital and electron densities are allowed to relax to the molecular equilibrium situation. The orbital interaction between PX_3 and [M@Au_{12}]^q can be viewed as the consequence of two main contributions: σ-donation from the σ-HOMO of PX_3 to the first virtual orbital of [M@Au_{12}]^q (mainly of a_g* type) and π-back-donation mainly involving the h_g HOMO of [M@Au_{12}]^q and the first virtual π-orbital of PX_3.

Sometimes, the two terms ΔE_{pauli} and ΔE_{elstat} are added up as ΔE_{st}, which is the so-called steric energy term.[50−52] But ΔE_{st} can have positive or negative values and have no physical sense in having an attractive steric interaction.[53,54] Since usually ΔE_{pauli} is repulsive and ΔE_{elstat} is attractive, the two terms may largely cancel each other, and the focus of the discussion of the bonding interactions then rests on the orbital interaction term ΔE_{orb}. This term can be partitioned into contributions from the different fragment orbital belonging to different irreducible representations of the interacting system. The complex [M@Au_{12}]$^q PX_3$ has C_s symmetry, which gives only a′ and a″ symmetries. One component of the near-degenerate [M@Au_{12}]$^q PX_3$ π-orbital belongs to a″, the other one to a′, which is also the symmetry of the σ-orbital. Therefore we define the σ and π contributions as follows: $\Delta E_\pi = 2\Delta E_{orb}(a'')$ and $\Delta E_\sigma = \Delta E_{orb}(a') - \Delta E_{orb}(a'')$.

TABLE 1: Optimized Geometric Parameters[a] for the W@Au$_{12}$PX$_3$ Complexes

	PF_3	PH_3	$P(OMe)_3$	PMe_3
R_{P-X}	1.584	1.424	1.623	1.838
R_{P-X} (free ligand)	1.598	1.434	1.649	1.858
R_{Au-W} (axial)	2.788	2.785	2.788	2.808
R_{Au-W} (equatorial)	2.738	2.741	2.732	2.721
θ_{X-P-X}	98.1	97.3	107.1	103.4
θ_{X-P-X} (free ligand)	97.8	91.8	105.7	99.5
R_{P-Au}	2.262	2.315	2.313	2.345
ΔE_b	−26.0	−27.5	−32.0	−38.4

[a] Bond lengths in Å, bond angles in deg, and energy in kcal/mol. The R_{Au-W} (in W@Au$_{12}$) is 2.734 Å.

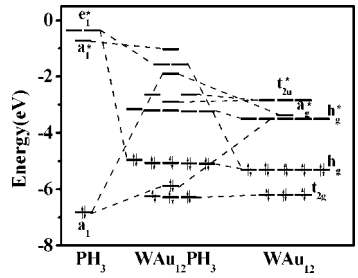

Figure 3. Correlation diagram of the frontier orbital of PH_3 and W@Au$_{12}$ forming W@Au$_{12}$PH$_3$.

3.2. W@Au$_{12}$PX$_3$ (X = H, F, Cl, Br, I, Me, OMe). ***3.2.1. W@Au$_{12}$PH$_3$.*** Figure 2 presents the geometries of the free ligand PH_3 (C_{3v}) of W@Au$_{12}$ (I_h) and of the W@Au$_{12}$PH$_3$ complex (always kept in C_s). Comparison of the geometries gives interesting information about the changes induced by Au−P bond formation. The P−H bonds of PH_3 in the complexes are ∼1 pm shorter than that in free PH_3. Au→PH_3 π-back-donation takes place into the P−H π* antibonding orbital, which is expected to lengthen the P−H bonds. So some other effects must cause the P−H bond shortening.

The first one is the change in hybridization of the P−H bonds. Upon Au−P bond formation, the lone-pair donor orbital of P looses some s and achieves more p character, while more s character is left over for the hybridized P−H bonds. According to Bent's rule,[55] this leads to shorter P−H bonds. At the same time, we can note the θ_{H-P-H} bond angles of the PH_3 ligand in the complexes are 5.5° larger than those in free PH_3, which corroborates the explanation.

The second effect comes from the change of the atomic partial charge of P in the complexes, which becomes more positive because of the P→Au charge donation. The higher positive charge at the P atom induces H→P charge donation, which may also lead to shorter P−H bonds in the complexes. As seen from R_{P-H} and Δq(P) in Table 5, we can come to the conclusion too.

Figure 3 is the correlation diagram of the frontier orbital of PH_3 and W@Au$_{12}$ forming W@Au$_{12}$PH$_3$. In terms of the orbital shapes interaction rule, the a_1 HOMO of PH_3 mainly interacts with the LUMO+1 a_g* of W@Au$_{12}$ to form a top site σ-type orbital rather than with h_g* LUMO of W@Au$_{12}$. This makes the axial Au−W bonds significantly longer than the equatorial bonds in W@Au$_{12}$.

3.2.2. W@Au$_{12}$PX$_3$ (X = H, F, Me, OMe). The optimized geometry parameters are summarized in Table 1. The calculations show a positive correlation between the Au−P bond lengths and the bond energies (k_{kor} > 0.8). The most strongly bonded ligand, PMe_3, yields the longest M−PX_3 bonds. The long M−PMe_3 bonds are not caused by steric repulsion between the methyl subsistent and the W@Au$_{12}$ cluster. This becomes evident by comparing the bond angles θ_{X-P-X} (X = Me, H), which are larger for Me than for H. That longer bonds may be stronger has been mostly explained by the electrostatic term ΔE_{elstat}. Table 3 shows that the largest difference in the three terms (ΔE_{pauli}, ΔE_{elstat} and ΔE_{orb}) between PH_3 and PMe_3 is ΔE_{elstat} (−136.2 and −157.9kcal/mol), which leads to the final difference of ΔE_b (−27.5 and −38.5kcal/mol). Of course, the metal−ligand interactions have also contributions from P→M σ-donor and M→P π-back-bonding orbital interactions. It is therefore difficult to predict if a longer donor/acceptor bond is weaker or stronger than a shorter bond.

TABLE 2: Composition of the P Lone-Pair Orbital and the P−X Bond Orbital in Free PX_3 and in Complexes W@Au$_{12}$PX$_3$[a]

model		PF_3	PH_3	$P(OMe)_3$	PMe_3
free ligand	% s(P)$_{LP}$	76.0	51.7	67.8	53.7
	% p(P)$_{LP}$	24.0	48.2	32.2	46.3
	% s(P and X)$_{BD}$	20.5	57.3	22.0	22.1
	% p(P and X)$_{BD}$	79.0	42.3	77.4	77.6
	q(P)	1.63	−0.05	1.49	0.83
W@Au$_{12}$PX$_3$	% s(P)$_{LP}$	39.7	36.4	32.9	27.1
	% p(P)$_{LP}$	60.0	63.5	66.8	72.9
	% s(P and X)$_{BD}$	24.5	57.7	26.6	25.3
	% p(P and X)$_{BD}$	75.1	41.9	72.9	74.4
	$\Delta q(PX_3)$	0.17	0.15	0.28	0.22
	$\Delta q(X_3)$	0.05	0.11	0.11	0.15
	Δq(P)	0.12	0.04	0.17	0.07
	Δq_σ(P)	0.68	0.62	0.78	0.77
	Δq_π(P)	−0.56	−0.58	−0.61	−0.70

[a] q: atomic partial charge. LP: lone-pair orbital. BD: bonding orbital. Δ: difference between free and bonded ligand. Negative numbers indicate increases in electronic charges, positive numbers indicate decreases in electronic charges.

The results of NBO analysis are given in Table 2. The s and p character of the phosphorus lone-pair orbital is different in the different free ligands and shows no correlation with the bond energy, but there is a nice correlation in the complexes, obviously reduced with s character. The lone-pair orbital acquires much more p character in the complexes where the percent of s(P) contribution is clearly lower than the percent of p(P) contribution.

The PX_3 ligand carries a positive charge throughout, i.e. they are electron donors as expected. The NBO-partial charges of the PX_3 ligand show for all metals the somewhat unexpected trend $P(OMe)_3$ > PMe_3 > PF_3 > PH_3. PF_3 is actually a stronger charge donor than PH_3, and $P(OMe)_3$ a stronger one than PMe_3. Note that the distances between the phosphorus and the gold atom (R_{P-Au}) in PF_3 and $P(OMe)_3$ are shorter than these in PH_3 and PMe_3. The shorter distance can lead to the stronger orbital interaction and more electron transfer. The separation of the M←PX_3 charge donation into contributions by P and by X shows that the intraligand charge exchange plays a significant role. The charge donations $\Delta q(X_3)$ in PMe_3 and PH_3 are even higher than the donation of the P atom, but there is the opposite case in $P(OMe)_3$ and PF_3 (Table 2). Thus, a significant part of the charge donation of PMe_3 and PH_3 comes from the substituents X.

Δq_σ(P) donation and Δq_π(P) back-donation are both large, but the σ donor property is stronger than the π acceptor tendency. The π-acceptor strength increases in the same order as the phosphane bond energy compared in Tables 1 and 2.

3.2.3. Bond Energy Analysis of W@Au$_{12}$PX$_3$ (X = H, F, Cl, Br, I, Me, OMe). Table 3 presents the results of the bond energy analysis of the phosphane complexes.

The largest contribution to the M−PX_3 bond energy ΔE_b for all complexes comes from the term ΔE_{pauli}, the overlap repulsion of the P lone-pair and the Au closed core shells. ΔE_{pauli} is

TABLE 3: Results of Bond Energy Analysis (Energy in kcal/mol) of $W@Au_{12}PX_3$ (X = H, F, Cl, Br, I, Me, OMe)

	PF_3	PCl_3	PBr_3	PI_3	PH_3	$P(OMe)_3$	PMe_3
ΔE_{prep}	0.64	0.36	0.36	0.43	1.34	1.40	2.44
ΔE_{int}	−26.7	−24.8	−24.4	−25.7	−28.8	−33.5	−40.8
ΔE_{pauli}	170.5	154.8	149.5	139.5	166.4	172.1	179.2
ΔE_{elstat}	−126.2 (64.0%)	−113.5 (63.2%)	−106.1 (61.0%)	−98.4 (59.6%)	−136.2 (69.8%)	−141.1 (68.6%)	−157.9 (71.8%)
ΔE_{orb}	−71.0 (36.0%)	−66.1 (36.8%)	−67.8 (39.0%)	−66.8 (40.4%)	−59.0 (30.2%)	−64.5 (31.2%)	−62.1 (28.2%)
ΔE_σ	−39.4	−38.0	−39.7	−40.1	−39.7	−45.1	−45.4
ΔE_π	−31.7	−28.1	−28.1	−25.9	−19.3	−19.4	−16.6
$\Delta E_\sigma/\Delta E_\pi$	1.24	1.35	1.42	1.55	2.05	2.33	2.73
ΔE_b	−26.0	−24.5	−24.0	−25.2	−27.5	−32.0	−38.5

TABLE 4: Results of Bond Energy Analysis (Energy in kcal/mol) of $[M@Au_{12}]^qPH_3$ ($M^q = Hf^{2-}$, Ta^-, W, Re^+, Os^{2+}, Ir^{3+}, Pt^{4+}, Au^{5+})

	$M^q =$							
	Hf^{2-}	Ta^-	W	Re^+	Os^{2+}	Ir^{3+}	Pt^{4+}	Au^{5+}
ΔE_{prep}	0.38	0.33	1.34	2.23	3.78	5.57	8.96	15.2
ΔE_{int}	−13.9	−19.5	−28.8	−40.2	−53.9	−70.6	−90.2	−117.0
ΔE_{pauli}	183.1	168.9	166.4	159.3	147.1	140.3	137.3	128.1
ΔE_{elstat}	−140.7 (71.4%)	−133.5 (70.1%)	−136.2 (69.8%)	−135.2 (67.8%)	−130.3 (64.8%)	−129.3 (61.3%)	−130.8 (57.5%)	−129.0 (52.6%)
ΔE_{orb}	−56.3 (28.6%)	−54.9 (29.9%)	−59.0 (30.2%)	−64.3 (32.2%)	−70.7 (35.2%)	−81.6 (38.7%)	−96.7 (42.5%)	−116.1 (47.4%)
ΔE_σ	−32.9	−34.2	−39.7	−46.5	−54.7	−66.0	−80.2	−98.4
ΔE_π	−23.4	−20.6	−19.3	−17.8	−16.1	−15.6	−16.5	−17.7
$\Delta E_\sigma/\Delta E_\pi$	1.40	1.66	2.05	2.61	3.40	4.23	4.87	5.57
ΔE_b	−13.5	−19.1	−27.5	−38.0	−50.1	−65.0	−81.3	−101.8

overcompensated by electrostatic and orbital interaction attractions, with negatively larger ΔE_{elstat} than ΔE_{orb}. It suggests more electrostatic than covalent character. Throughout, the σ energy contribution is larger than the π term. In terms of the ratio of ΔE_π to ΔE_σ, the phosphanes were classified into three groups by Branchadell.[22] PMe_3, PPh_3, and $P(i\text{-}Pr)_3$ were considered as σ-donor ligand, PH_3, and $P(OMe)_3$ as intermediate cases, and PF_3 and $P(NC_4H_4)_3$ as σ-donor/π-acceptor ligand. In Figure 4, the correlation of the Pauling electronegativities of these X substituents and the ratio of ΔE_π to ΔE_σ was given by our work. The $\Delta E_\sigma/E_\pi$ values of these complexes become lower with the increase of the Pauling electronegativities of these X substituents. The differences are found for the $P(OMe)_3$ and PMe_3 complexes because of the difference between group and single atom. So according to these results, it can be concluded that the donor/acceptor ratio increases for different X substituents in the order $F < Cl < Br < I < H < OMe < Me$. Just this order was found by Branchadell[22] in an energy decomposition analysis of $Fe(CO)_5PR_3$ though the author only used the frontier orbital interactions as σ and π contributions.

3.3. $[M@Au_{12}]^qPH_3$ ($M^q = Hf^{2-}$, Ta^-, W, Re^+, Os^{2+}, Ir^{3+}, Pt^{4+}, Au^{5+}). ***3.3.1. Bond Energy Analysis of $[M@Au_{12}]^qPH_3$ ($M^q = Hf^{2-}$, Ta^-, W, Re^+, Os^{2+}, Ir^{3+}, Pt^{4+}, Au^{5+}).*** Table 4 presents the results of the bond energy analysis of the phosphane complexes $[M@Au_{12}]^qPH_3$ ($M^q = Hf^{2-}$, Ta^-, W, Re^+, Os^{2+}, Ir^{3+}, Pt^{4+}, Au^{5+}). The trends of the different energy terms, ΔE_{pauli}, ΔE_{elstat}, ΔE_{orb}, and ΔE_b, are displayed in Figure 5.

Figure 5 shows that ΔE_{pauli}, ΔE_{orb}, and the bond energy ΔE_b all decrease, and ΔE_{elstat} increases approximately, with an increase of nuclear and cluster charge. The ΔE_{elstat} term is always larger than the ΔE_{orb} term. This means that the $[M@Au_{12}]^q-PH_3$ bonding in this series of complexes is more electrostatic than covalent. There is an interesting point that comes out of the energy analysis. Table 4 shows that the charge of the metal cluster has very little effect on the electrostatic interaction between the two fragments. And the proportion of the electrostatic interaction in both attractive components decreases with the increase of the charge of the cluster. This means that the higher charged complexes have the smaller degree of electrostatic bonding. From the trend of the frontier orbital energy levels in Figure 6, the highest charged complex (Au_{13}^{5+}) has the lowest LUMO, which leads to the strongest orbital interactions, especially in the electron acceptor. Thus, the charge of the metal clusters has a larger effect on the covalent bonding through its lowering of the orbital energy levels than on the electrostatic interactions.

The analysis of the metal−PH_3 interactions makes it possible to give other explanations about the trends. The large positive charge of the quintuple charged Au_{13}^{5+} causes the metals to become very good electron attractors. The total charge transfer from the P atom to the metal cluster is very large, as seen from Table 5. ΔE_b decreases with the increase of the charge of the cluster while the ability of the cluster strengthens as an electron acceptor.

It is also shown in Table 4 that the stabilization due to $[M@Au_{12}]^q\leftarrow PH_3$ σ-donation steadily increases from $[Hf@Au_{12}]^{2-}$ to Au_{13}^{5+}, while the $[M@Au_{12}]^q\leftarrow PH_3$ π-back-donation exhibits the opposite trend (Pt^{4+} and Au^{5+} are a little abnormal). But the absolute numbers for σ-donation and π-back-donation are not very meaningful. The ratio of σ-donation and π-back-donation energies exhibits a gradual increase from $[Hf@Au_{12}]^{2-}$ to Au_{13}^{5+}. The trends can be explained with the lowering of the orbital energies of the h_g HOMO and a_1 LUMO+1 of $[M@Au_{12}]^q$ from $[Hf@Au_{12}]^{2-}$ to Au_{13}^{5+}. Figure 6 shows that the energy levels of the frontier orbital of $[M@Au_{12}]^q$, the very low lying σ LUMO+1 of Au_{13}^{5+}, and the very high lying π HOMO of $[Hf@Au_{12}]^{2-}$ explain why the $[M@Au_{12}]^q\leftarrow PH_3$ σ-donation in the $Au_{13}^{5+}PH_3$ and the $[M@Au_{12}]^q\rightarrow PH_3$ π-back-donation in the $[Hf@Au_{12}]^{2-}PH_3$ have the biggest values. The same trend was found in an energy decomposition analysis of $TM(CO)_6^q$ by Frenking.[32]

It becomes obvious from Table 5 that the largest π-back-donation from the occupied d orbital of the metal into the $\pi^*_{(P-H)}$ orbital leads to a longer P−H bond, which becomes quite long in $[Hf@Au_{12}]^{2-}PH_3$. On the contrary, there are much shorter P−H bonds in $[Ir@Au_{12}]^{3+}PH_3$, $[Pt@Au_{12}]^{4+}PH_3$, and

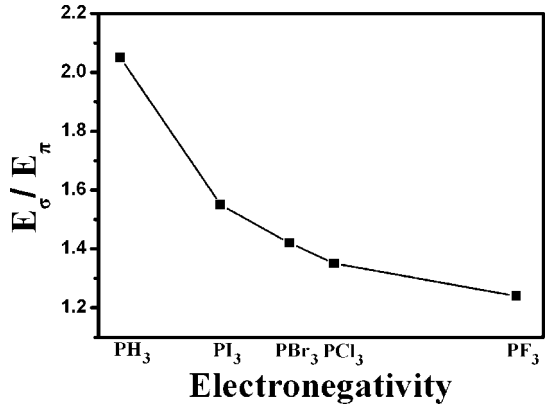

Figure 4. Relationship of the $\Delta E_\sigma/\Delta E_\pi$ (donor/acceptor) ratio of PX_3 as the X's Pauling electronegativitiy.

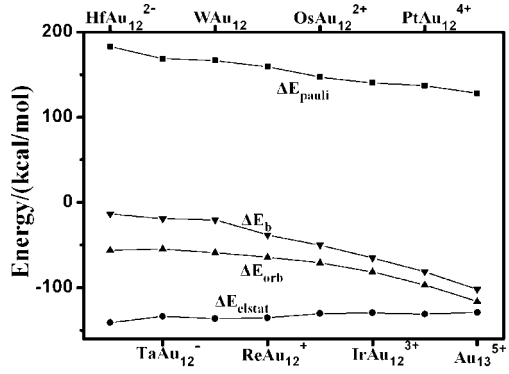

Figure 5. Trend of the energy contributions to the interaction energy between $[M@Au_{12}]^q$ and PH_3.

TABLE 5: Optimized Geometric Parameters and the NBO Analysis of $[M@Au_{12}]^q$ PH_3[a]

	M^q =							
	Hf^{2-}	Ta^-	W	Re^+	Os^{2+}	Ir^{3+}	Pt^{4+}	Au^{5+}
R_{P-H}	1.440	1.429	1.424	1.419	1.416	1.413	1.417	1.414
θ_{H-P-H}	93.2	94.8	97.3	98.9	100.6	102.6	104.8	107.4
R_{P-Au}	2.326	2.329	2.315	2.315	2.332	2.345	2.354	2.377
$\Delta q(P)$[b]	−0.04	−0.03	−0.01	0.00	0.03	0.06	0.09	0.18

[a] Bond lengths in Å, bond angles in deg. [b] Differences of the partial charges between the free ligand and the bonded ligand; positive numbers indicate decreases in electronic charges of the bonded ligand.

$Au_{13}^{5+}PH_3$, which have the dominant $PH_3 \rightarrow [M@Au_{12}]^q$ σ-donation in the bonding forces.

3.3.2. Effect on $[M@Au_{12}]^qPH_3$ (M^q = Hf^{2-}, W, Ir^{3+}) by Changing the Au−P Distance. From earlier calculations of $Cr(CO)_6$ reported by Sherwood and Hall,[56] which discussed the correlation between the Cr−CO distance and the C−O bond length, we know that π-back-donation and σ-donation are two reverse factors affecting the C−O bond lengths. Because of the similar distribution of orbital electron in CO and PH_3 (their HOMO and LUMO are all the $\sigma_{C-O}/\sigma_{P-H}$ and π^*_{C-O}/π^*_{P-H}, respectively), we can suppose that the M−PH_3 distance is correlative with the P−H bond length too. The P−H distance decreases and the P−H stretching frequency increases first as a result of $PH_3 \rightarrow [M@Au_{12}]^q$ σ-donation when a PH_3 ligand approaches a metal cluster. But $[M@Au_{12}]^q \rightarrow PH_3$ π-back-donation becomes effective at a shorter M−PH_3 distance, which leads to a turning point along the M−PH_3 coordinate. This is because the overlap of the σ orbitals, which are aligned along the internuclear axis, starts earlier than the overlap of the π orbitals, which are orthogonal to the σ bonding. The overlap of the σ orbitals has a maximum value at a certain M−PH_3 distance, and becomes smaller at shorter distances.

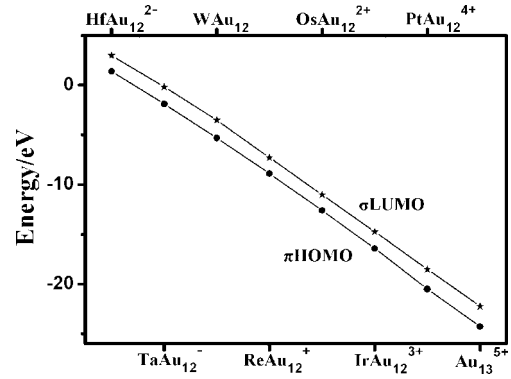

Figure 6. Trend of the frontier orbital energy levels of the $[M@Au_{12}]^q$.

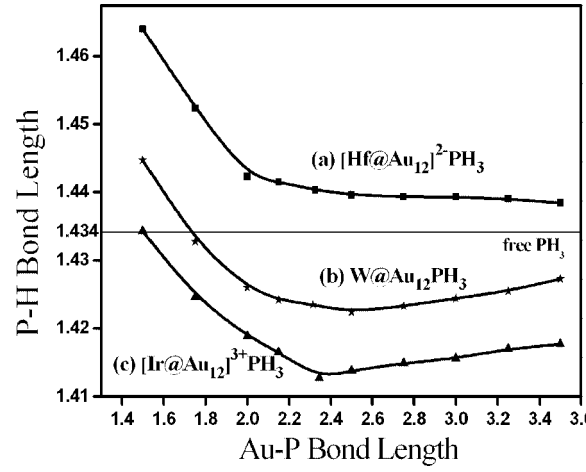

Figure 7. Calculated P−H bond lengths as a function of the Au−P distance: (a) $[Hf@Au_{12}]^{2-}PH_3$; (b) $W@Au_{12}PH_3$; and (c) $[Ir@Au_{12}]^{3+}PH_3$. Bond lengths in Å.

To investigate the P−H bond length of a PH_3 as a function of the TM−PH_3 distance, $[Hf@Au_{12}]^{2-}PH_3$, $W@Au_{12}PH_3$, and $[Ir@Au_{12}]^{3+}PH_3$ as examples, we have optimized the P−H bond length at different Au−P distances (see Figure 7). Figure 7a shows that the P−H bond of $[Hf@Au_{12}]^{2-}PH_3$ becomes shorter at longer Au−PH_3 distances, but it never becomes shorter than in free PH_3. This result is apparently in conflict with the calculations of SH,[56] which predict shorter C−O bond lengths at longer metal−CO distances. However, the HOMO of the dianion $[Hf@Au_{12}]^{2-}$ is very diffuse because it is occupied by two weakly bonded electrons which have been added to the neutral compound. The $[Hf@Au_{12}]^{2-} \rightarrow PH_3$ π-back-donation can therefore compete with the $H_3P \rightarrow [Hf@Au_{12}]^{2-}$ σ-donation even at longer Au−P distances. Table 6 shows that the $[Hf@Au_{12}]^{2-} \rightarrow PH_3$ π-back-donation and the $H_3P \rightarrow [Hf@Au_{12}]^{2-}$ σ-donation decrease at longer Au−P distances but the ratio of the two components remains nearly the same until the bond is stretched by up to 3.0 Å. There is still a significant contribution of the π-back-donation when the bond is further stretched by up to 3.5 Å. The very long reach of the $[Hf@Au_{12}]^{2-} \rightarrow PH_3$ π-back-donation explains why there is a smooth decrease and no turning point of the P−H bond length when the Au−P distance becomes longer.

Figure 7b also shows the results for $W@Au_{12}PH_3$. Unlike the case for $[Hf@Au_{12}]^{2-}PH_3$, there is a turning point in P−H distance when the Au−P distance is slightly longer than that at

TABLE 6: Calculated P−H Bond Lengths R_{P-H} (Å), ΔE_σ and ΔE_π (kcal/mol), and Back-Donation ($\Delta E_\pi/\Delta E_{orb}$) as a Function of the Au−P Distance[a]

	R_{Au-P} =									
	1.50	1.75	2.00	2.15	eq[a]	2.50	2.75	3.00	3.25	3.50
					$[Hf@Au_{12}]^{2-}PH_3$					
R_{P-H}	1.464	1.452	1.442	1.443	1.440	1.440	1.439	1.439	1.439	1.438
ΔE_σ	−115.0	−86.4	−60.2	−46.0	−32.8	−23.0	−13.0	−7.4	−4.4	−2.5
ΔE_π	−188.7	−105.9	−56.2	−38.1	−23.4	−14.5	−7.5	−3.9	−2.0	−1.4
$\%\Delta E_\pi/\Delta E_{orb}$	62.1	55.1	48.3	45.3	41.6	38.7	36.4	34.5	31.1	35.5
					$W@Au_{12}PH_3$					
R_{P-H}	1.445	1.433	1.426	1.424	1.424	1.422	1.423	1.424	1.426	1.427
ΔE_σ	−109.7	−85.7	−63.3	−51.0	−39.7	−29.2	−18.6	−11.5	−7.0	−4.1
ΔE_π	−173.1	−93.5	−47.9	−31.5	−19.3	−11.1	−5.1	−2.4	−1.2	−0.6
$\%\Delta E_\pi/\Delta E_{orb}$	61.2	52.2	43.1	38.2	32.7	27.6	21.7	17.3	14.3	12.8
					$[Ir@Au_{12}]^{3+}PH_3$					
R_{P-H}	1.434	1.425	1.419	1.417	1.413	1.414	1.415	1.416	1.417	1.418
ΔE_σ	−119.9	−103.9	−87.0	−77.3	−66.0	−57.9	−46.8	−37.5	−30.4	−25.0
ΔE_π	−160.0	−82.3	−40.9	−26.8	−15.6	−10.4	−5.8	−3.7	−2.7	−2.1
$\%\Delta E_\pi/\Delta E_{orb}$	57.2	44.2	32.0	25.7	19.1	15.2	11.1	9.0	8.1	7.8

[a] Au−P distance at the equilibrium geometry: 2.326 Å for $[Hf@Au_{12}]^{2-}PH_3$, 2.315 Å for $W@Au_{12}PH_3$, and 2.345 Å for $[Ir@Au_{12}]^{3+}PH_3$.

the equilibrium geometry. The result for $W@Au_{12}PH_3$ is in agreement with the previous study of SH.[56] The bond energy analysis results given in Table 6 show that the contribution of the M→PH_3 π-back-donation of the neutral complex displays a steeper decrease than for $[Hf@Au_{12}]^{2-}PH_3$.

The result for $[Ir@Au_{12}]^{3+}PH_3$ is similar with that for $W@Au_{12}PH_3$. There is a turning point on the curve at the equilibrium geometry (see Figure 7c). After this, the P−H bond becomes longer but it cannot approach the value for free PH_3 even when the Au−P distance is stretched by up to 3.5 Å. Thus, $[Ir@Au_{12}]^{3+}PH_3$ is an example for the case which has the shorter P−H bond length than the value for free PH_3, even though the Au−P distance is stretched very long because of the large positive charge. Table 6 shows that the relative contribution of the π-back-donation decreases when the Au−P distance becomes longer. At the distance of 3.5 Å there is only 7.8% $[Ir@Au_{12}]^{3+}$→PH_3 π-back-donation left.

According to Bent's rule,[55] the R_{P-H} of the complex $[M@Au_{12}]^qPH_3$ should decrease with the increase of the charge of $M@Au_{12}$ while the θ_{H-P-H} should increase. Table 5 shows the trends well. In this scene, the dominating reason is that the charge of teh P atom becomes less and less from $[Hf@Au_{12}]^{2-}$ to Au_{13}^{5+}. Accordingly, it will induce H→P charge donation, which may also lead to shorter P−H bonds in the complexes.

4. Summary and Conclusion

Concerning the $W@Au_{12}PX_3$ and $[M@Au_{12}]^qPH_3$ complexes with different transition metals M, charges q, and PX_3 ligands, we may draw the following conclusions.

1 There is some soft correlation between the bond lengths and bond energies of the Au−P bonds of the $W@Au_{12}PX_3$ (X = H, F, Cl, Br, I, Me, OMe) systems. The bonding energy ΔE_b between $W@Au_{12}$ and PX_3 ligands follows the trend PMe_3 < $P(OMe)_3$ < PH_3 < PF_3 ≈ PI_3 ≈ PCl_3 ≈ PBr_3, while the Au−PX_3 interatomic distances decrease in the series PMe_3 > PH_3 ≈ $P(OMe)_3$ > PF_3.

2 The energy decomposition analysis indicates that the σ-donor/π-acceptor ratios increase for different X substituents with the decrease of their Pauling electronegativities.

3 The different transition metals (M^q = Hf^{2-}, Ta^-, W, Re^+, Os^{2+}, Ir^{3+}, Pt^{4+}, Au^{5+}) in $[M@Au_{12}]^q$ become more prone to combine with PH_3 with the increase of the charge q. There is a regular decrease of the ratio of metal→PH_3 π-back-donation in the same order.

4 The P−H bond length in $[M@Au_{12}]^qPH_3$ (M = Hf^{2-}) decreases smoothly when PH_3 approaches the metal cluster. However, for M = W and Ir^{3+}, a turning point in the optimized P−H distance shows up when the Au−P distance is slightly longer than at equilibrium.

Acknowledgment. We acknowledge financial support by the National Nature Science Foundation of China (No. 20573074) and the SRFDP of China (No. 20040248017).

References and Notes

(1) Haruta, M. *Catal. Today* **1997**, *36*, 153.
(2) Andres, R. P.; Bein, T.; Dorogi, M.; Feng, S.; Henderson, J. L.; Kubiak, C. P.; Mahoney, W.; Osifchin, R. G.; Reifenberger, R. *Science* **1996**, *272*, 1323.
(3) Andres, R. P.; Bielefeld, J. D.; Henderson, J. L.; Janes, D. B.; Kolagunta, V. R.; Kubiak, C. P.; Mahoney, W. J.; Osifchin, R. G. *Science* **1996**, *273*, 1690.
(4) Schwerdtfeger, P. *Angew. Chem., Int. Ed.* **2003**, *42*, 1892.
(5) Garzón, I. L.; Michaelian, K.; Beltrán, M. R.; Posada-Amarillas, A.; Ordejón, P.; Artacho, E.; Sánchez-Portal, D.; Soler, J. *M. Phys. Rev. Lett.* **1998**, *81*, 1600.
(6) Wang, J. L.; Wang, G. H.; Zhao, J. J. *Phys. Rev. B* **2002**, *66*, 035418.
(7) Oviedo, J.; Palmer, R. E. *J. Chem. Phys.* **2002**, *117*, 9548.
(8) Pyykkö, P.; Runeberg, N. *Angew. Chem., Int. Ed.* **2002**, *41*, 2174.
(9) Pyykkö, P. *Chem. Rev.* **1988**, *88*, 563.
(10) Scherbaum, F.; Grohmann, A.; Huber, B.; Krüger, C.; Schmidbaur, H. *Angew. Chem., Int. Ed. Engl.* **1988**, *27*, 1544.
(11) Pyykkö, P. *J. Org. Chem.* **2006**, *691*, 4336.
(12) Autschbach, J.; Hess, B. A.; Johansson, M. P.; Neugebauer, J.; Patzschke, M.; Pyykkö, P.; Reiher, M.; Sundholm, D. *Phys. Chem. Chem. Phys.* **2004**, *6*, 11.
(13) Li, X.; Kiran, B.; Li, J.; Zhai, H. J.; Wang, L. S. *Angew. Chem., Int. Ed.* **2002**, *41*, 4786.
(14) Zhai, H. L.; Li, J.; Wang, L. S. *J. Chem. Phys.* **2004**, *121*, 8369.
(15) Frenking, G. *J. Organomet. Chem.* **2001**, *635*, 9.
(16) Dewar, M. J. S. *Bull. Soc. Chim. Fr.* **1951**, *18*, C79.
(17) Chatt, J.; Duncanson, L. A. *J. Chem. Soc.* **1953**, 2929.
(18) Ruiz-Morales, Y.; Ziegler, T. *J. Phys. Chem. A* **1998**, *102*, 3970.
(19) Xiao, S. X.; Trogler, W. C.; Ellis, D. E.; Berkovitch-Yellin, Z. *J. Am. Chem. Soc.* **1983**, *105*, 7033.
(20) Marynick, D. S. *J. Am. Chem. Soc.* **1984**, *106*, 4064.
(21) Bowmaker, G. A.; Schmidbaur, H.; Krüger, S.; Rösch, N. *Inorg. Chem.* **1997**, *36*, 1754.
(22) González-Blanco, Ò.; Branchadell, V. *Organometallics* **1997**, *16*, 5556.
(23) Dapprich, S.; Frenking, G. *Organometallics* **1996**, *15*, 4547.

(24) Fernandez, A. L.; Wilson, M. R.; Prock, A.; Giering, W. P. *Organometallics* **2001**, *20*, 3429.
(25) Frenking, G.; Wichmann, K.; Fröhlich, N.; Grobe, J.; Golla, W.; Le Van, D.; Krebs, B.; Läge, M. *Organometallics* **2002**, *21*, 2921.
(26) Wang, S. P.; Richmond, M. G.; Schwartz, M. *J. Am. Chem. Soc.* **1992**, *114*, 7595.
(27) Alyea, E. C.; Song, S. Q. *Inorg. Chem.* **1995**, *34*, 3864.
(28) Willner, H.; Aubke, F. *Angew. Chem., Int. Ed. Engl.* **1997**, *36*, 2402.
(29) Lupinetti, A. J.; Jonas, V.; Thiel, W.; Strauss, S. H.; Frenking, G. *Chem. Eur. J.* **1999**, *5*, 2573.
(30) Lupinetti, A. J.; Fau, S.; Frenking, G.; Strauss, S. H. *J. Phys. Chem. A* **1997**, *101*, 9551.
(31) Mavridis, A.; Harrison, J. F.; Allison, J. *J. Am. Chem. Soc.* **1989**, *111*, 2482.
(32) Diefenbach, A.; Bickelhaupt, F. M.; Frenking, G. *J. Am. Chem. Soc.* **2000**, *122*, 6449.
(33) Szilagyi, R. K.; Frenking, G. *Organometallics* **1997**, *16*, 4807.
(34) Reed, A. E.; Curtiss, L. A.; Weinhold, F. *Chem. Rev.* **1988**, *88*, 899.
(35) Morokuma, J. *J. Chem. Phys.* **1971**, *55*, 1236.
(36) Kitaura, K.; Morokuma, K. *Int. J. Quantum Chem.* **1976**, *10*, 325.
(37) Uddin, J.; Frenking, G. *J. Am. Chem. Soc.* **2001**, *123*, 1683.
(38) Lein, M.; Frunzke, J.; Timoshkin, A.; Frenking, G. *Chem. Eur. J.* **2001**, *7*, 4155.
(39) Te Velde, G.; Bickelhaupt, F. M.; Baerends, E. J.; Guerra, C. F.; Van Gisbergen, S. J. A.; Snijders, J. G.; Ziegler, T. *J. Comput. Chem.* **2001**, *22*, 931.
(40) Gunnarsson, O.; Lundqvist, B. I.; Wilkins, J. W. *Phys. Rev. B* **1974**, *10*, 1319.
(41) Vosko, S. H.; Wilk, L.; Nusair, M. *Can. J. Phys.* **1980**, *58*, 1200.
(42) Perdew, J. P.; Wang, Y. *Phys. Rev. B* **1992**, *45*, 13244.
(43) Perdew, J. P.; Chevary, J. A.; Vosko, S. H.; Jackson, K. A.; Pederson, M. R.; Singh, D. J.; Fiolhais, C. *Phys. Rev. B* **1992**, *46*, 6671.
(44) Van Lenthe, E.; Baerends, E. J.; Snijders, J. G. *J. Chem. Phys.* **1993**, *99*, 4597.
(45) Van Lenthe, E.; Baerends, E. J. *J. Comput. Chem.* **2003**, *24*, 1142.
(46) Rosén, A.; Lindgren, I. *Phys. Rev.* **1968**, *176*, 114.
(47) Andrae, D.; Haeussermann, U.; Dolg, M.; Stoll, H.; Preuss, H. *Theor. Chim. Acta* **1990**, *77*, 123.
(48) Ditchfield, R.; Hehre, W. J.; Pople, J. A. *J. Chem. Phys.* **1971**, *54*, 724.
(49) Frisch, M. J.; Trucks, G. W.; Schlegel, H. B.; Scuseria, G. E.; Robb, M. A.; Cheeseman, J. R.; Montgomery, J. A.; Vreven, T.; Kudin, K. N.; Burant, J. C.; Millan, J. M.; Iyengar, S. S.; Tomasi, J.; Barone, V.; Mennucci, B.; Cossi, M.; Scalmani, G.; Rega, N.; Petersson, G. A.; Nakatsuji, H.; Hada, M.; Ehara, M.; Toyota, K.; Fukuda, R.; Hasegawa, J.; Ishida, M.; Nakajima, T.; Honda, Y.; Kitao, O.; Nakai, H.; Klene, M.; Li, X.; Knox, J. E.; Hratchian, H. P.; Cross, J. B.; Bakken, V.; Adamo, C.; Jaramillo, J.; Gomperts, R.; Stratmann, R. E.; Yazyev, O.; Austin, A. J.; Cammi, R.; Pomelli, C.; Ochterski, J. W.; Ayala, P. Y.; Morokuma, K.; Voth, G. A.; Salvador, P.; Dannenberg, J. J.; Zakrzewski, V. G.; Dapprich, S.; Daniels, A. D.; Strain, M. C.; Farkas, O.; Malick, D. K.; Rabuck, A. D.; Raghavachari, K.; Foresman, J. B.; Ortiz, J. V.; Cui, Q.; Baboul, A. G.; Clifford, S.; Cioslowski, J.; Stefanov, B. B.; Liu, G.; Liashenko, A.; Piskorz, P.; Komaromi, I.; Martin, R. L.; Fox, D. J.; Keith, T.; Al-Laham, M. A.; Peng, C. Y.; Nanayakkara, A.; Challacombe, M.; Gill, P. M. W.; Johnson, B.; Chen, W.; Wong, M. W.; Gonzalez, C.; Pople, J. A. *GAUSSIAN 03*; Gaussian, Inc., Wallingford, CT, 2004.
(50) Ziegler, T.; Tschinke, V.; Becke, A. D. *J. Am. Chem. Soc.* **1987**, *109*, 1351.
(51) Ziegler, T.; Tschinke, V.; Ursenbach, C. *J. Am. Chem. Soc.* **1987**, *109*, 4825.
(52) Li, J.; Schreckenbach, G.; Ziegler, T. *J. Am. Chem. Soc.* **1995**, *117*, 486.
(53) Frenking, G.; Wichmann, K.; Fröhlich, N.; Loschen, C.; Lein, M.; Frunzke, J.; Rayón, V. M. *Coord. Chem. Rev.* **2003**, *238*−*239*, 55.
(54) Dykstra, C. E.; Frenking, G.; Kim, K. S.; Scuseria, G. E. *Theory and applications of Computational Chemistry*; Elsevier: Boston, MA, 2005; p 291.
(55) Bent, H. A. *Chem. Rev.* **1961**, *61*, 275.
(56) Sherwood, D. E.; Hall, M. B. *Inorg. Chem.* **1983**, *22*, 93.

JP808403U